Tribology Letters (2022) 70:85
https://doi.org/10.1007/s11249-022-01625-z

TRIBOLOGY METHODS

A Novel Set-Up for In Situ Measurement and Mapping of Lubricant Film Thickness in a Model Rolling Bearing Using Interferometry and Ratiometric Fluorescence Imaging

Mourad Chennaoui[1,2] · Mark Fowell[1,3] · He Liang[1,4] · Amir Kadiric[1]

Received: 3 May 2022 / Accepted: 6 June 2022
© The Author(s) 2022

Abstract
This paper describes a unique experimental set-up constructed for studies of lubricant behaviour in an operating rolling element bearing including in situ quantitative measurements of film thickness in and around the element-raceway contact. The set-up is based on a deep groove ball bearing in which the outer race is made of sapphire to allow full optical access to the zone in which the rolling elements are loaded against it. This allows direct imaging of lubricant films under both steady-state and transient conditions and at contact pressures and rotational speeds representative of those present in real rolling element bearings. Optical interferometry is used to measure thin EHL films inside the ball–raceway contacts while a specific laser induced fluorescence approach, referred to as ratiometric fluorescence, is implemented to observe the lubricant distribution and quantify its thickness ahead of the ball–raceway contact. Results are presented to validate the accuracy of the method and to investigate the influence of bulk lubricant viscosity and bearing speed on contact film thickness, inlet starvation and lubricant distribution around the ball–raceway contact. To the best of our knowledge, the work described here is the first to directly measure lubricant distribution and EHL film thickness in a ball–raceway contact in an operating radial rolling bearing.

✉ Amir Kadiric
a.kadiric@imperial.ac.uk

[1] Tribology Group, Imperial College London, London SW7 2AZ, UK

[2] Present Address: SKF RTD, Houten, the Netherlands

[3] Present Address: Volvo Trucks, Gothenburg, Sweden

[4] Present Address: School of Mechanical Engineering, Beijing Institute of Technology, Beijing, China

Published online: 01 July 2022

Graphical Abstract

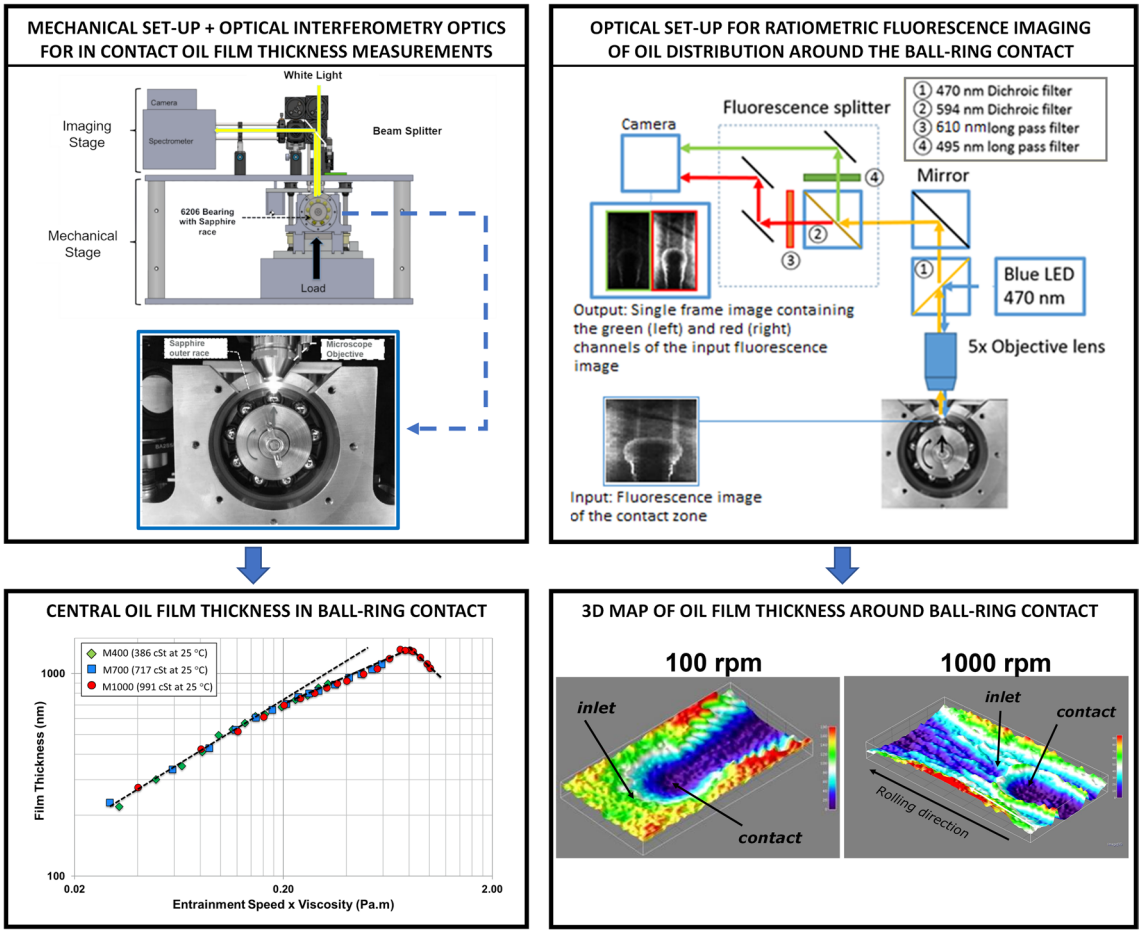

Keywords Rolling bearing · Elastohydrodynamic lubrication (EHL) · Ratiometric laser-induced fluorescence (LIF) · Inlet film · Starvation · Ultrathin film interferometry

1 Introduction

The thickness of the elastohydrodynamic film [1–5] formed between the rolling elements and raceways of a rolling bearing is a key parameter determining the performance and durability of the bearing. It determines the extent to which the rolling elements and raceways are separated by a lubricant film and hence plays a major role in determining the friction, wear and rolling contact fatigue life of rolling bearings. In consequence, numerous experimental techniques have been developed to measure film thickness in rolling bearing-type contacts, with the most widely used being optical interferometry [6–8], capacitance [9, 10], ultrasound [11, 12] and fluorescence [13–16]. These techniques are normally applied to a single contact configuration where the contact itself is stationary, commonly a ball-on-disc set-up, rather than an actual rolling bearing, since this makes it relatively straight-forward to access the contact, to control the surface speeds and applied load, and to extract and interpret measurements. The optical interferometry-based techniques of ultra-thin film interferometry [7, 17] and the relative optical interference intensity [8, 18] have been widely used to measure the film thickness in ball-on-disc contacts down to 2 nm with a precision of ± 1 nm. Laser induced fluorescence has also been employed relatively extensively to measure film thickness present between two surfaces, again in single contacts [16, 19]. Its main advantages over interferometry techniques is that it can measure much thicker films, in the range of a few microns as opposed to the maximum of a few 100 s of nanometres for optical interferometry, and requires no reflective coating on specimens; however, it suffers from a major disadvantage of being unable to measure the very thin films of 10 s of nanometres and less which commonly occur in non-conformal tribological contacts such as those in

rolling bearings. Given their respective measurement ranges, these two techniques are complementary and together they cover film thicknesses from a few nanometres to a few microns.

Studies of lubricant film thickness in actual rolling bearings where there are multiple, moving element-raceway contacts are much rarer. Ultrasound reflection method has been used to measure film thickness in real bearings [20–22]; however, measurements were only possible at relatively slow bearing speeds since the element-ring contact must be in position long enough for an ultrasound pulse to reflect. Capacitance has also been employed to measure film thickness in deep groove ball bearings by replacing all but one of the steel balls by electrically-insulating ceramic balls [23–25]. Thin film sputtered transducers have been developed that are able to measure capacitance between an individual ball and raceway during bearing operation [26], but these are quite difficult to apply to surfaces, are fragile and require local electrical access. A few studies have used optical interferometry to measure film thickness in rolling bearings. Badahoran et al. [27] employed interferometry to measure film thickness in a cylindrical roller bearing at low loads using a quartz glass outer raceway while Ohno et al. [28] measured the film thickness in a thrust ball bearing where one of the washers was made of sapphire and was flat. Both studies used counter-rotation where the raceways were driven in opposite directions, so as to fix the positions of the rolling elements in space so that a stationary or very slow-moving individual contacts could be studied.

Clearly, the ability to measure film thickness in actual rolling element bearings under realistic operating conditions would offer an important step forward in our understanding of bearing lubrication given that several factors are at play in an operating bearing that are not present in a single-contact configuration. In addition to the EHL film thickness in the element-ring contacts, it is important to be able to study the actual distribution of lubricant in a bearing. It is well-known that in-contact elastohydrodynamic film thickness is determined by the amount of lubricant present in the contact inlet region and that when this is constrained starvation can ensue, leading to a reduction of elastohydrodynamic film thickness [29–34]. In fact, our understanding of EHL film behaviour when the contact inlet is fully flooded is well developed so that determining the inlet supply conditions is arguably the biggest challenge in practical situations. In rolling element bearings, the lubricant distribution and hence this inlet supply is thought to depend on several factors including the lubricant properties, cage design and the number and spacing of rolling elements, since there is limited time for lubricant reflow into the raceway tracks between over-rollings. Noda et al. [35] applied X-Ray CT imaging to explore the distribution of grease in a rolling bearing made from resin, while Franken et al. [36] used fluorescence spectroscopy to map the circumferential distribution of grease around a bearing using optical access from the side, but apart from these, very little experimental data exists concerning the distribution of lubricant in operating rolling bearings.

In this article, we describe a novel experimental set-up that enables a direct observation of lubricant distribution and measurement of lubricant film thickness in a model ball bearing at realistic bearing speeds and loads. To achieve this the set-up employs a deep groove ball bearing where the outer bearing raceway has been replaced by a sapphire ring to enable optical access in and around the ball–raceway contact. The EHL film thickness in ball–raceway contacts is measured with nanometre accuracy using optical interferometry while the distribution of lubricant outside of the contacts including its thickness in the inlet to the ball–raceway contact, is mapped using ratiometric fluorescence imaging. Lubrication conditions are studied over a bearing speed range from 100 to 3000 rpm and ball–ring Hertz contact pressure of 1.6 GPa. The measured EHL central film thickness is related to the mapped lubricant volume in the inlet over a range of conditions, with both being compared to existing predictions from elastohydrodynamic lubrication models.

2 Sapphire Bearing Rig Design

2.1 Hardware Layout

The sapphire bearing rig (SBR) consists of two stages, a mechanical stage and an imaging stage, as shown schematically in Fig. 1. The mechanical stage comprises a housing to support and locate the bearing, an electric motor that drives the bearing inner ring via a flexible coupling and the loading system. The load is applied via a stepper motor pushing onto a load lever arm which then pushes the shaft/inner ring assembly directly upwards hence loading it against the outer ring. This loading system is very similar to that found on the well-established MTM ball-on-disc tribometer. The shaft/inner ring assembly is mounted on a set of low friction, precision linear guides ensuring that the load is always acting directly upwards. The most highly loaded ball in this set-up is, therefore, the one at the uppermost point of the bearing. The bearing ring housing contains a tapered cut-out in this region to accommodate a microscope objective and allow optical access to the loaded contact of the ball and the outer sapphire ring as evident in Fig. 1. In the current study a standard 6206 deep groove ball bearing was used with the outer AISI 52100 steel raceway replaced by a sapphire ring. The sapphire ring was especially manufactured for this purpose by an external supplier with very tight tolerances on surface finish, to ensure good quality images, as well as on concentricity and cylindricity. The inner and outer diameter

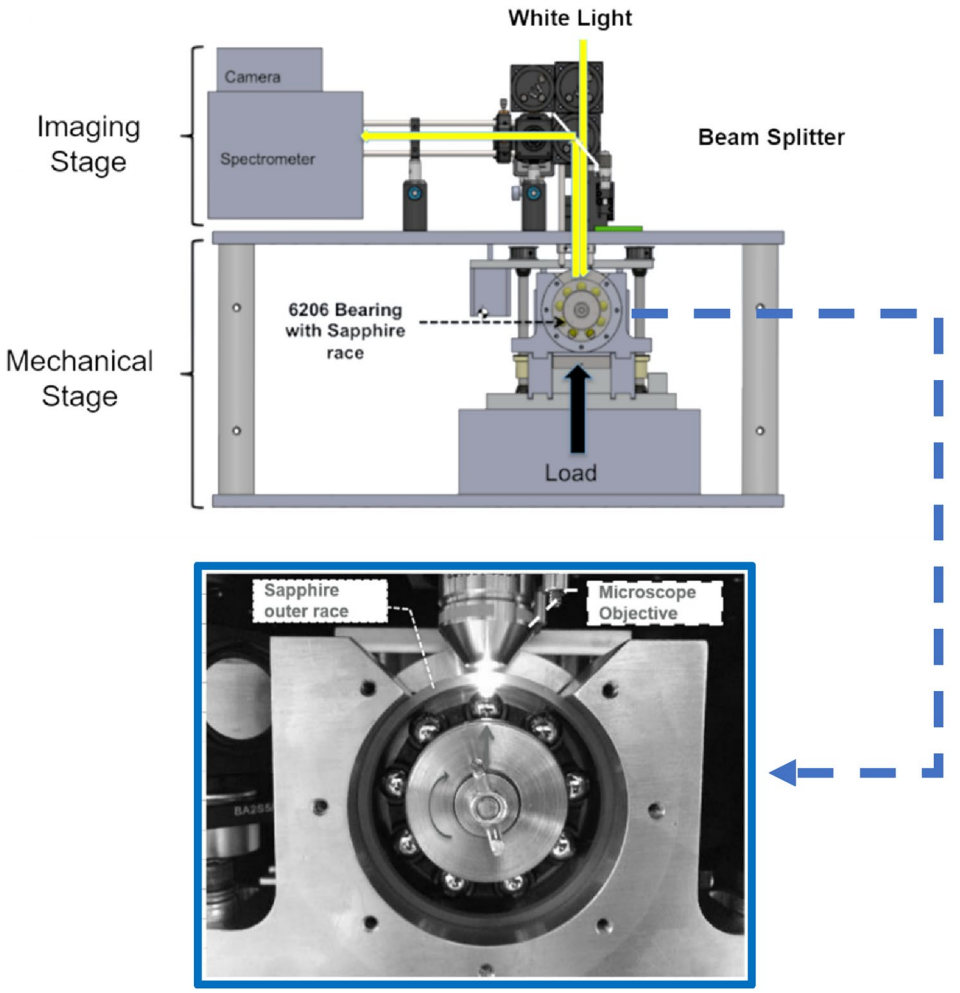

Fig. 1 Top: An illustration showing the main aspects of the sapphire bearing rig (SBR) in interferometry mode. Bottom: A close up photograph of the bearing and the location of the microscope objective used for imaging (Color figure online)

surfaces were finished with an optical polish quality of 80/50 scratch/dig per MIL13830 specifications. Cylindricity of inner diameter was better than 0.025 mm and concentricity better than 0.1 mm. To enable oil film measurements with optical interferometry (see later), a chromium layer of 20 nm in thickness and the SiO_2 layer of 520 ± 25 nm in thickness were deposited on the inner diameter of the ring. The radial variation in coating thickness was 1 nm/mm. The coatings were deposited using custom made tooling to achieve these specifications. In the present set-up the sapphire ring is cylindrical i.e. it has no curvature in the direction transverse to rolling unlike the original steel raceway. This is due to difficulties in manufacturing such a curvature in sapphire while still ensuring the optical quality and cylindricity of the sapphire ring. The bearing housing also contains the oil bath at the bottom which, once filled, provides dip lubrication to the bearing. The oil fill level is measured using a scale attached to the outside of the housing. The temperature of the oil sump and at the outer ring location as close as possible to the area being imaged is monitored using thermocouples. The uppermost EHL contact formed between the steel ball and the sapphire outer raceway is imaged using a $5\times$ microscope objective (Zeiss).

The imaging stage is modular so that the SBR can be operated with either the ultrathin film interferometry or a fluorescence measurement stage and these can be interchanged without disturbing the mechanical setup and test conditions. Figure 1 shows the SBR with the interferometry stage in place. Each imaging stage comprises an illumination source (mercury lamp for interferometry and LED for fluorescence) together with the various optical elements (lenses, mirrors and fluorescence filters) that focus and direct light into the contact zone and gather it toward the imaging components (tube lens, spectrometer, fluorescence imaging splitter, camera). Further relevant details of the optical set-up are described in the interferometry and fluorescence sections below.

One of the important aspects of the SBR optical set-up is that it must be able to capture the relevant image extremely quickly to minimise blurring which can occur due to the fast movement of the contact through the field of view. The time taken for the contact to move across the field of view

is dependant on the bearing geometry, its rotational speed and the width of the ball–outer raceway contact which is determined by the applied bearing load. For example, for the bearing speed of 3000 rpm and Hertz pressure in the ball–outer raceway contact of 1.6 GPa, the contact transit time in the SBR set-up is about 21 ms. The exposure time needs to be much shorter than this to minimise blurring, ideally it should be short enough to capture the image in a time shorter than the contact transverses a distance equivalent to a single pixel. For this reason, the camera employed in the SBR (Andor, iStar 334 T series, UK; an intensified gated camera) is specifically chosen to be able to capture good quality images in a very short exposure time. The minimum exposure time for the camera employed is specified as 5 ns although in the present experiments there was no need to use exposure times quite as short as this.

2.2 Triggering System

In standard single contact ball-on-disc test rigs, the contact formed between the ball and the disc is stationary relative to the field of view of the optical system. By contrast, in a rolling bearing where the outer ring is stationary, the contact passes momentarily through the field of view due to rotation of the ball assembly around the bearing. Therefore, a fast and stable triggering mechanism is required to ensure adequate synchronisation between the spatial position of the balls and the timing of the image capture. Triggering must enable that at any given bearing speed, the image is captured when a ball passes the uppermost point of the bearing.

To achieve this, a low power diode laser is directed to a selected ball from the side of the bearing and the reflected beam used to trigger the optical system. When the apex of a ball passes through a specific position it reflects the incident light beam at the conjugate angle to the angle of incidence. A photo-detector comprising a narrow spatial filter and thresholding is used to detect the beam and create a digital TTL pulse signal. In operation, balls are detected at a set angle, α, in advance of the field of view (uppermost point) and an adjustable delay time *dt* is applied to the pulse signal to trigger image acquisition precisely when the contact is in the correct position with respect to the field of view, either exactly central to it when measuring EHL film thickness or just behind the centre when measuring films in the contact inlet. The time *dt* is determined by angle α and the speed of ball assembly, v namely $dt = R_o\ \alpha/v$, where R_o is the radius of the outer ring. As the bearing speed rises from 100 to 3000 rpm in a test, the delay time decreases from *dt* to only 1/30 *dt*. The angle α should thus be selected so that the delay time is not too small at 3000 rpm but at 100 rpm is less than the interval between two adjacent balls. An angle in the range 5°–10° was found to be suitable.

The way that triggering is employed differs between the optical interferometry and the fluorescence modes of measurement. When ultra-thin film interferometry is used, the triggering pulse is used to activate the camera that captures an image from the spectrometer, as indicated in Fig. 2. By contrast, in fluorescence measurement mode, the triggering pulse is used to activate the excitation LED. This is because there is an upper limit to how long and how intensely the contact zone can be illuminated before fluorescence photobleaching and saturation [37, 38] adversely affect the quality of the measurements.

2.3 Ultra-thin Film Interferometric Stage

The ultra-thin film interferometry method is fully described in [7] and since its invention has been widely applied to single-contact EHL film thickness measurements. It combines the use of a spectrometer and a spacer layer on top of a thin semi-reflective coating deposited on the transparent counterface. In the SBR, a lubricated contact is formed between a reflective steel ball and a transparent sapphire raceway. The inner surface of the transparent raceway (the lubricant side) is coated with a 20 nm thick semi-reflective chromium coating on top of which is deposited a transparent SiO_2 spacer layer of thickness 520 ± 25 nm. The precise spacer layer thickness in the imaging location is determined from a stationary contact at the start of a test. White light is shone through the transparent raceway into the contact where some of it is immediately reflected from the semi-reflective coating. The remainder passes through the spacer layer and any lubricant film present before being reflected from the steel ball. When these two beams recombine they experience optical interference due to the optical path difference resulting from the passage of one of them through the spacer layer and lubricant film. A spectrometer is then used to determine the wavelengths of maximum constructive or destructive interference, from which this optical path difference and thus the sum of the spacer layer and lubricant film thickness can be determined. In the SBR, a mercury lamp is used to provide a high intensity, broadband white light. The details of the optical set-up used for the interferometry measurements together with the triggering system described above are shown in Fig. 2.

2.4 Fluorescence Imaging Setup

In the simplest form of laser-induced fluorescence (LIF), a fluorescent dye is dissolved in the lubricant and a monochromatic light source (a laser or an LED) having a frequency that activates the fluorescent molecular groups is shone into the contact. Provided that a number of factors are satisfied, in particular that excitation light intensity is significantly lower than the saturation intensity of the chosen dye, the

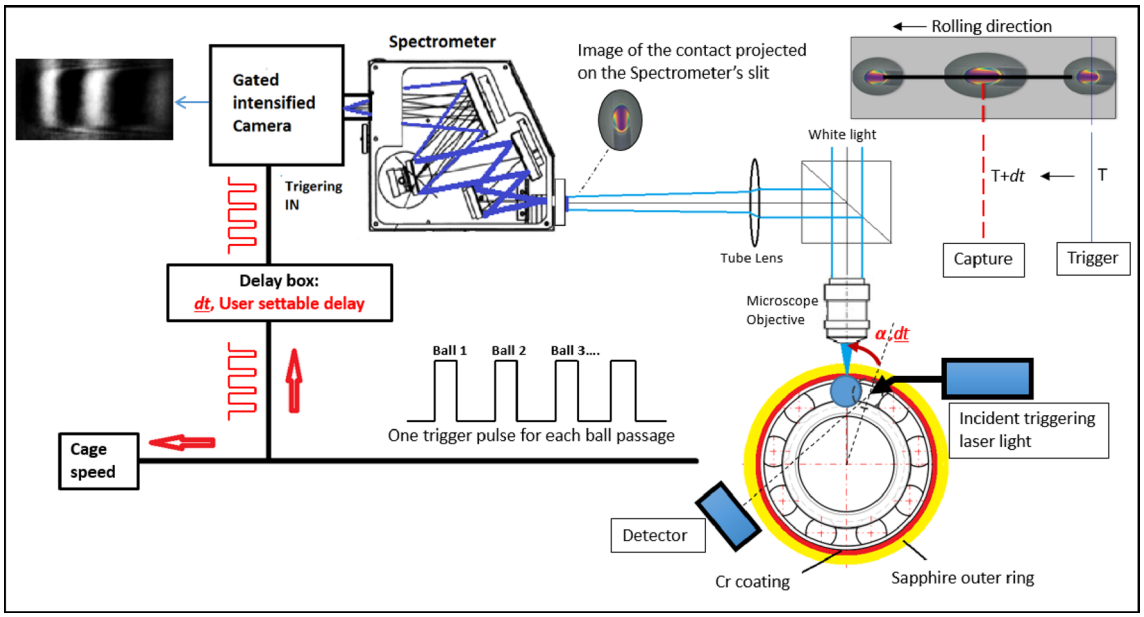

Fig. 2 A diagram illustrating the optical setup of the ultra-thin film interferometry technique and the triggering system used in the Sapphire Bearing Rig (Color figure online)

intensity of the resulting fluorescence signal emitted is proportional to the number of fluorescent molecules present and is thus proportional to the lubricant film thickness. The relationship between the fluorescence emission intensity, $I_f(l)$ and the cross-sectional thickness of the probed volume (i.e. the film thickness), (l) can be expressed as:

$$I_f(l) \approx I_0 \phi \varepsilon_{\lambda_{ex}} Cl,$$

where I_0 is the intensity of the excitation light at wavelength λ_{ex}, f is the dye's quantum efficiency (the ratio of photons absorbed to the photons emitted through fluorescence), $\varepsilon_{\lambda_{ex}}$ is the molar extinction coefficient of the dye, and C is the concentration of the dye dissolved in the fluid.

A major limitation of this simple approach is that its accuracy is dependent on the intensity of the exciting light signal being constant over time. In the SBR, this condition cannot be satisfied since the time for which the contact is within the excitation field depends on the rotational speed. An additional complication in application of standard fluorescence to SBR is that during bearing rotation the excitation light incidence angle on the contact zone changes with the spatial position of the ball during its passage through the contact zone. These SBR specific variabilities compound the one due to any temporal instability of the excitation light intensity which is present in the standard application of fluorescence too. To address these potential sources of inaccuracies, a novel application of ratiometric laser-induced fluorescence imaging for measurement of lubricant film thickness in a rolling bearing was employed here. Ratiometric LIF was originally developed by Hidrovo and Hart [39] who referred to it as emission reabsorption laser induced fluorescence (ERLIF) and demonstrated its ability to measure oil thickness in a gap between two stationary quartz plates in the range 5–400 mm with 1% accuracy. A detailed description of the ratiometric fluorescence technique implemented here and the benefits it offers over the standard LIF approach are described in the Appendix to this paper. The reader is referred to the Appendix for full details but in brief, the technique uses two fluorescent dyes dissolved in the lubricant, a "donor" dye, D and an "acceptor" dye, A. If there is spectral overlap between the donor dye and acceptor dye, photons emitted by excited molecules of D excite the molecules of A. This leads to quenching of the fluorescence emission of D in the spectral overlap region while the emission intensity of A is almost unchanged since the donor excitation is negligible compared to its direct excitation. The ratio of the fluorescence signals of D and A then correlates linearly with the film thickness regardless of the original excitation intensity. This ratiometric approach also avoids other experimental problems such as optical non-linearities, surface reflectivity and temporal variations in excitation source intensity.

The optical set-up required for the successful application of the ratiometric LIF imaging in the SBR is rather complex. Its main aspects are illustrated in Fig. 3 which shows a sketch of the SBR in the fluorescence mode (top) and the detail of the optical paths for the ratiometric fluorescence imaging (bottom). The lubricant is tagged with two dyes, which in the present study were Pyrromethene 546, (P546) and Pyrromethene 650, (P650) acting as the donor and the acceptor dye, respectively. A 470 nm blue LED (M470L2, 1600 mA, Thorlabs) is employed as the excitation light source and this is triggered as a ball passes through the field

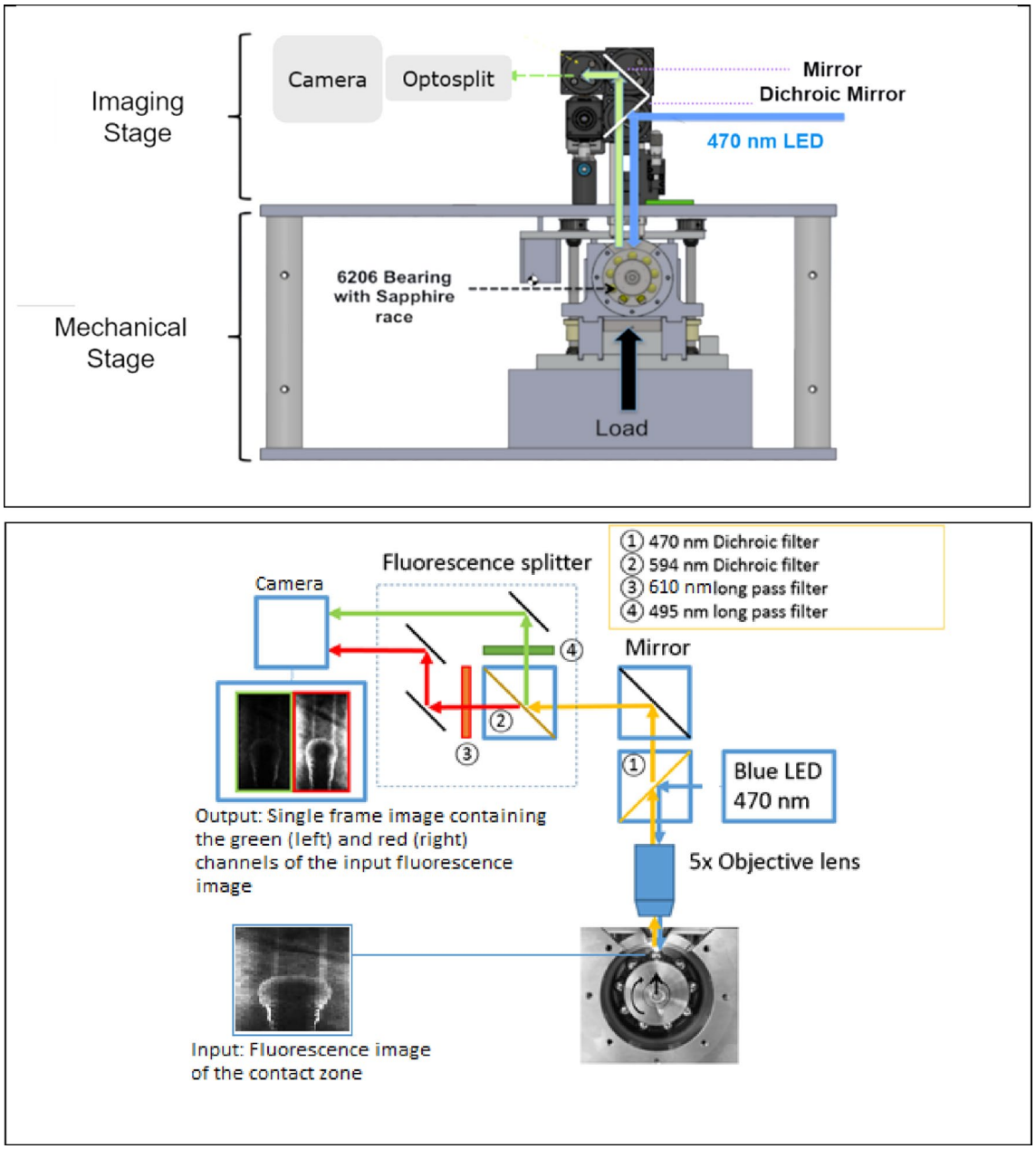

Fig. 3 A schematic diagram of the optical setup for the ratiometric laser induced fluorescence technique employed in the Sapphire Bearing Rig (SBR). Top: Hardware set-up of the SBR in the fluorescence mode; Bottom: Detail of the optical paths for the ratiometric fluorescence imaging (Color figure online)

of view. A fluorescence imaging splitter (Cairn, Optosplit II, UK) splits the fluorescence image of the contact zone into two channels: one for the donor dye (green in Fig. 3) and the other for the acceptor dye (red in Fig. 3). Channel segregation is achieved with a set of dichroic (marked as 1 and 2 in Fig. 3) and long pass filters (marked as 3 and 4 in Fig. 3) chosen so that emission signal overlap between the two dyes is minimised. An intensified gated camera (Andor, iStar 334 T series, UK), minimum exposure time of 5 ns, is connected to the output of the splitter so that it captures the emitted fluorescence as a single frame. The use of a single camera aids with the synchronisation of the images coming from the two channels. The captured two-channel image is subsequently split using software processing to form two separate images, one for each fluorescent channel, and these images are then superimposed and aligned in software. Once

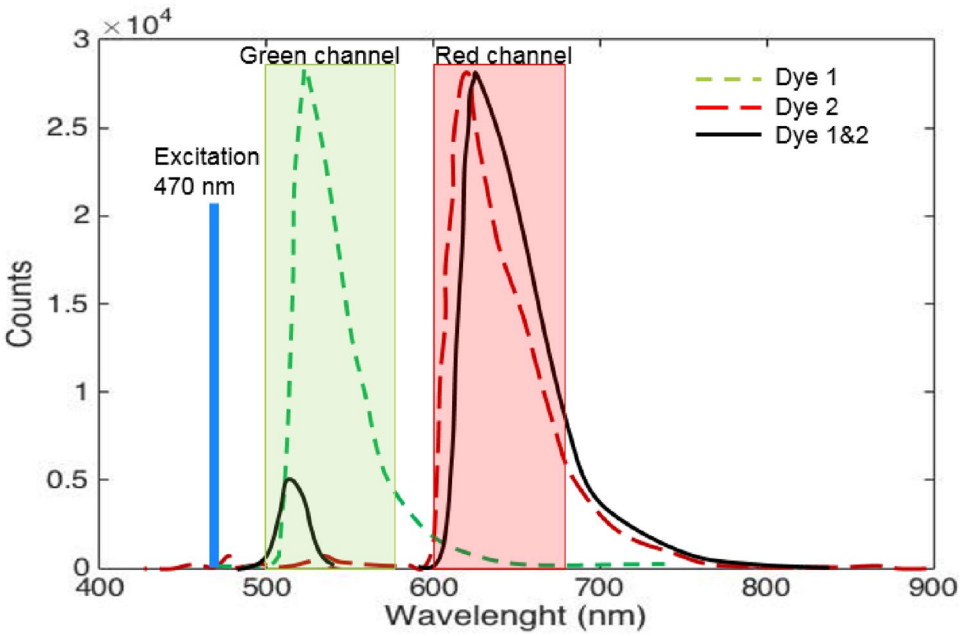

Fig. 4 An illustration of the ratiometric fluorescence principle using two dyes showing the emission spectrum of the donor dye 1 (green) and the acceptor dye 2 (red) and both dyes (black) when dissolved in the same base oil and excited by a 470 nm LED light. The two dyes used are Pyrromethene 546 and Pyrromethene 650, respectively (Color figure online)

the images are correctly registered, a pixel-wise division of intensity combined with the calibration curve (see later and Fig. 5) is used to give a pixel-wise map of the lubricant film thickness in the field of view, which in the present case was the inlet region of the ball–raceway contact. The use of a single camera also aids with the synchronisation of the image capture for the two channels.

2.5 Fluorescence Calibration

Figure 4 shows the emission spectra of the donor dye, P546, the acceptor dye, P650, and a mixture of both dyes in base oil. The maximum emission peaks are at wavelengths of ~ 540 nm and ~ 630 nm for P546 and P650 respectively. When the two dyes are mixed together and the lubricant excited at 470 nm, radiative transfer takes place from P546 to P650, resulting in quenching of the fluorescence emission of P546 in the spectral overlap region 550 to 600 nm. The emission intensity of P650 remains unchanged since the contribution of the radiative transfer to the overall emission signal of P650 is negligible compared to its direct excitation.

Theoretically, the recorded ratio of emission intensity of acceptor dye to donor dye should be proportional to the film thickness. To confirm this is true in the present implementation and to provide a film thickness calibration curve, fluorescence intensity ratios measured in the out-of-contact gap when a steel ball is loaded statically against the outer sapphire ring were plotted against the corresponding absolute film thickness values (i.e. height profile of this gap as calculated using Hertz contact theory [21] and also mapped using optical interference). The gap heights determined using these two methods were in close agreement. Figure 5 shows such a calibration of film thickness against ratiometric fluorescence intensity. It is evident that the relationship is linear for film thicknesses from 0.5 to more than 10 µm. The deviation from linearity increases for low film thicknesses, as is expected for fluorescence-based methods, and is about 10% at 0.5 µm film thickness. Therefore, 0.5 µm was taken to be the minimum lubricant layer thickness that can be measured reliably using the implemented ratiometric fluorescence technique. This minimum value is perfectly acceptable since fluorescence is here used to map lubricant distribution in the inlet region, where the lubricant layers are relatively thick, rather than to measure the very thin films within a contact for which the optical interferometry is used as described above. The two techniques complement each other and allow the present set-up to quantify lubricant film thicknesses both inside and outside of the ball–raceway contact.

3 Test Conditions and Lubricants

In the tests described in this study, the bearing rotational speed was varied from 100 to 2900 rpm, corresponding to entrainment speeds from 0.07 to 1.7 m/s at the ball–outer ring contact. The load was fixed at 50 N, giving a maximum Hertzian pressure of 1.57 GPa at the outer ring and the corresponding Hertzian contact dimensions of 196 µm and 172 µm in the rolling and transverse directions, respectively. The bearing was first run at the highest speed until the outer ring temperature measured near the imaging location reached an equilibrium value; film thickness measurements were then performed with

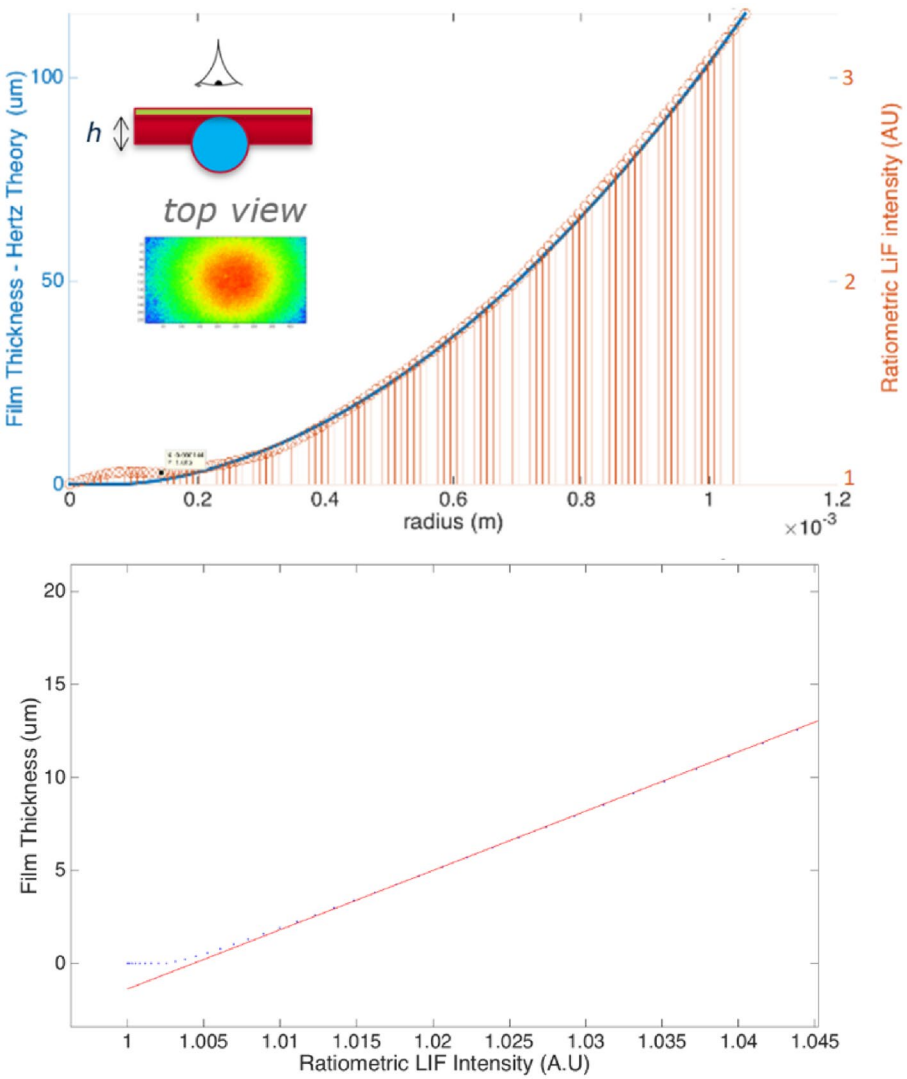

Fig. 5 Calibration data for the ratiometric fluorescence film thickness measurements. Top: A plot of ratiometric fluorescence signal (in arbitrary units) measured in the out-of-contact gap region when a steel ball is loaded statically against the sapphire outer ring with a load of 20 N versus the absolute height of that gap determined from the known contact geometry and Hertz theory. Top Inset: a schematic of the calibration setup and an example of a ratiometric fluorescence calibration image (The gap height plot shown in top figure is produced from such an image by taking an integrated line profile with a predetermined width from the centre of the contact and along its major width). Bottom: Fitted calibration curve between the absolute film thickness and the normalised ratiometric fluorescence intensity (minimum film thickness that can be measured with sufficient accuracy is taken from this plot to be 0.5 µm) (Color figure online)

Table 1 Viscosities of the test oils as measured at 25 °C

Lubricant	Viscosity (mPa s)	Density (kg/m^3)
M400	386	865
M700	717	871
M1000	991	871

descending speeds and the variation in the outer ring equilibrium temperature remained within 1 °C throughout the speed sweep. The equilibrium oil sump temperature was 32 °C in all tests.

Three Group 1 mineral base oils with different viscosities were used in the present tests. Their measured viscosities and densities at 25 °C are listed in Table 1. Relatively high oil viscosities were deliberately chosen in order to make it more likely for the onset of starvation in a bearing to be captured so that the reasons for it can be studied.

4 Results

4.1 Film Thickness in Ball–Ring Contacts

The EHL central film thickness in the loaded ball–sapphire outer ring contact was first measured using ultra-thin film interferometry. Measurements were conducted over a wide range of bearing speeds, from 100 to 2000 rpm for the two lower viscosity oils M400 and M700, and from 100 to 2900 rpm for the high viscosity oil M1000. All measurements were made at the bearing load of 50 N which equates to 1.57 GPa maximum Hertz pressure in the ball–sapphire ring contacts. The sump oil level was such that the lowest ball was submerged in oil to a half of its diameter.

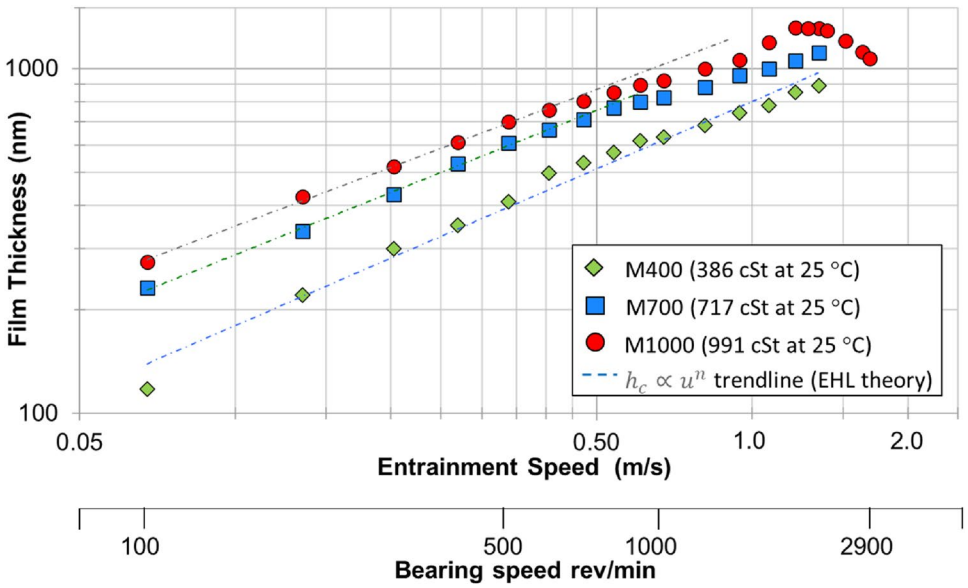

Fig. 6 Measured central film thickness in the ball–outer ring contact for the three test oils plotted against the contact entrainment speed and bearing rotational speed. Oil properties as given in Table 1, Max. Hertz pressure (ball–outer ring contact) = 1.57 GPa, Sump test temperarure = 32 °C (Color figure online)

Figure 6 shows film thickness measured in this way for the three test oils. For convenience, the x-axis in this plot shows both the bearing rotational speed and the corresponding entrainment speed in the ball–ring contact. The dashed lines show the $h_c \propto u^n$ trendlines i.e. a linear film vs speed relationship on a log–log plot as expected from EHL theory for fully flooded conditions. It is apparent that at relatively low speeds the measured film thickness increases linearly with speed on a log–log plot with a gradient of approximately 0.7 as expected from EHL theory. The absolute values of measured films are also found to be close to the theoretical ones. However, as the bearing speed is increased the measured film thicknesses start to fall below those of the linear trend. The film thickness is still increasing with speed but at lower rate than expected from EHL theory. The deviation is larger and occurs at lower speeds for the higher viscosity oils. For the lowest viscosity oil, M400, the film thickness starts to fall below the expected one at about 1200 rpm, for the intermediate viscosity oil, M700, this happens at about 900 rpm and for the highest viscosity oil, M1000, this is at around 700 rpm. Together, the trends described here indicate that there is some level of starvation occurring in the ball–ring contacts past certain bearing speed. The bearing speed at which the first onset of starvation occurs and the level of the resulting film reduction is determined by the oil viscosity. Additionally, with M1000 oil, where higher bearing speeds were tested (up to 2900 rpm), there is an actual decrease in film thickness with speed at speeds higher than 2000 rpm. This suggests that more severe starvation is now occurring so that as speed increases further the contact becomes more and more starved, leading to a negative trend in film thickness with speed as may be expected from starvation theory.

Figure 7 shows the same film thickness results now plotted against the product of lubricant viscosity and entrainment speed, ηu. This superimposes the curves for the three oils and shows clearly that the observed film thickness behaviour can be divided into three stages. At very small ηu values, the contact is fully flooded and the film thickness h_c is as predicted from fully flooded lubrication theory. At intermediate ηu values, the film thickness still increases with ηu but the discrepancy between the measured values and those predicted from fully flooded condition gets progressively larger as ηu increases. This suggests that some level of starvation is now occurring. At still higher ηu, the central film thickness h_c decreases at a rate proportional to u^{-1} which is in line with EHL starvation theory [31] and indicates that severe starvation may be occurring under these conditions.

4.2 Mapping of Oil Film Distribution in the Inlet of the Ball–Ring Contact

To further investigate the observed film thickness behaviour in the ball–ring contact, the oil film in the rolling track in the vicinity of the contact, including the inlet, was measured using the ratiometric fluorescence set-up on the sapphire bearing rig. The set-up allows for 3D maps of lubricant distribution all around the contact to be obtained. Typical such maps for the M1000 oil at three bearing speeds, 100, 1000 and 2000 rpm are shown in Fig. 8. It is evident that the imaging system enables good

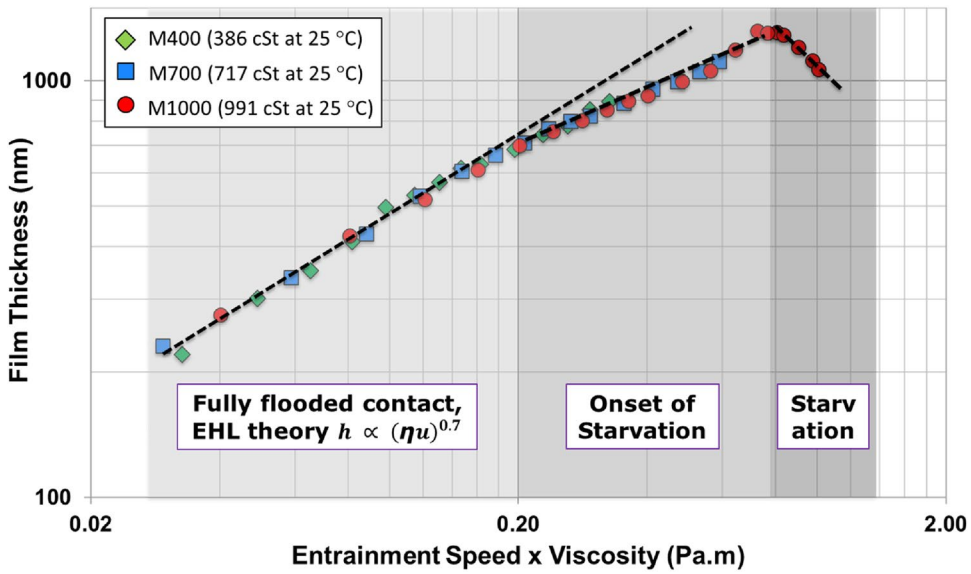

Fig. 7 Measured central film thickness in the ball–outer ring contact for the three test oils plotted against the product ηu; Same film thickness data as in Fig. 6 (Color figure online)

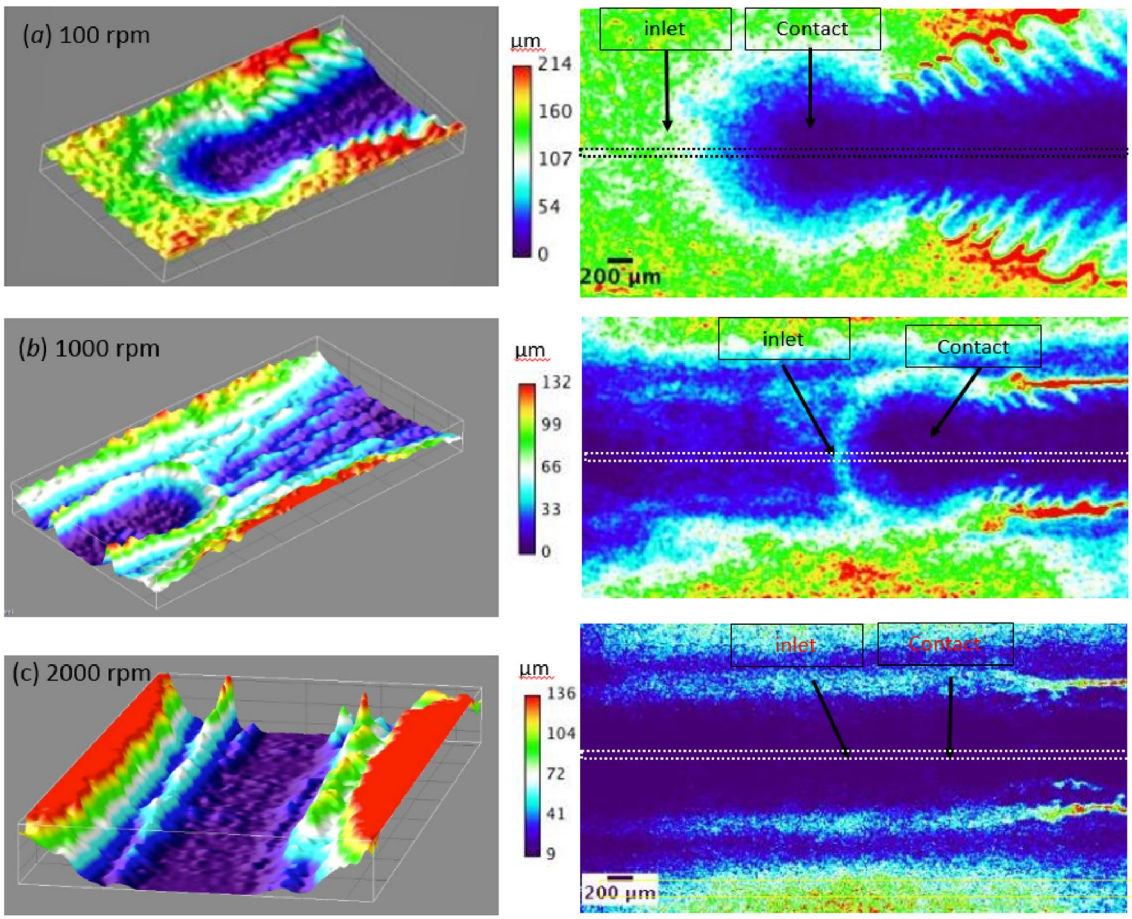

Fig. 8 Three-dimensional (left) and contour (right) maps of oil film thickness around the ball–outer ring contact including the inlet region for **a** 100 rpm, **b** 1000 rpm and **c** 2000 rpm. Oil M1000, Max. Hertz pressure (ball–outer ring contact) = 1.57 GPa, Sump test temperature = 32 °C; Locations of the contact and the inlet regions are as indicated in the images on the right (Color figure online)

quality maps of lubricant thickness to be obtained at a wide range of rolling speeds and over a large region surrounding the contact. The colour bar in each image indicates the quantitative values of the film thickness shown in the corresponding maps. The shapes of oil reservoir ahead of the contact can be seen clearly from the 3D plots allowing for quantitative assessment of the differences in the inlet oil supply at different speeds. At 100 rpm, which lies within the EHL theory region in Fig. 7, there is a large reservoir of oil in the rolling track and the inlet to the contact appears to be fully flooded (Fig. 8a). At 1000 rpm (within the onset of starvation region in Fig. 7) the oil reservoir ahead of the contact is visibly reduced (Fig. 8b). At 2000 rpm (within the starvation region in Fig. 7) there appears to be very little oil in the rolling track ahead of the ball–ring contact as indicated by the dark blue colour in the 3D map (Fig. 8c).

Figure 9 shows 2D profiles of the film thickness in the inlet region extracted from the 3D fluorescence maps along the dashed line in Fig. 8 i.e. along the centre of the contact in rolling direction with inlet on the left and outlet on the right. The thickness of this inlet film determines the amount of oil entrained into the contact and hence the in-contact film thickness shown earlier. The inlet film can be described using two parameters, the inlet distance from the front of the contact, S, where the oil starts to fill the inlet gap, and the thickness of the inlet film at this point, h_{oil}. Both of these are indicated in Fig. 9 for the present measurements. In fully flooded conditions, h_{oil} can be hundreds of times greater than the central film thickness, h_c, and S is of the order of contact width. In contrast, under starved conditions, the magnitude of h_{oil} approaches that of h_c and S approaches zero.

Figure 9 shows that at 100 rpm the inlet was fully flooded with oil. This is in line with the results shown in Figs. 6 and 7 where the central film thickness, h_c was measured to be in line with EHL theory. At 1000 rpm, the inlet film thickness, h_{oil} and meniscus distance, S were somewhat reduced, while at 2000 rpm, both h_{oil} and S were severely reduced indicating starved conditions, in line with the central film thickness measurements in Figs. 6 and 7.

Figure 10 plots the ratio of the measured central film thickness, h_c, to that predicted using EHL theory for fully flooded conditions, h_{cff}, against the non-dimensional inlet film thickness, h_{oil}/h_c. It is seen that central film thickness approached the predicted value (i.e. h_c/h_{cff} tends to 1) when inlet film was hundreds of times greater than the central film thickness but dropped further and further below the predicted value as the inlet film reduced i.e. as the ratio h_{oil}/h_c fell further below about 100. This general trend is in line with the results of starvation modelling [31, 32].

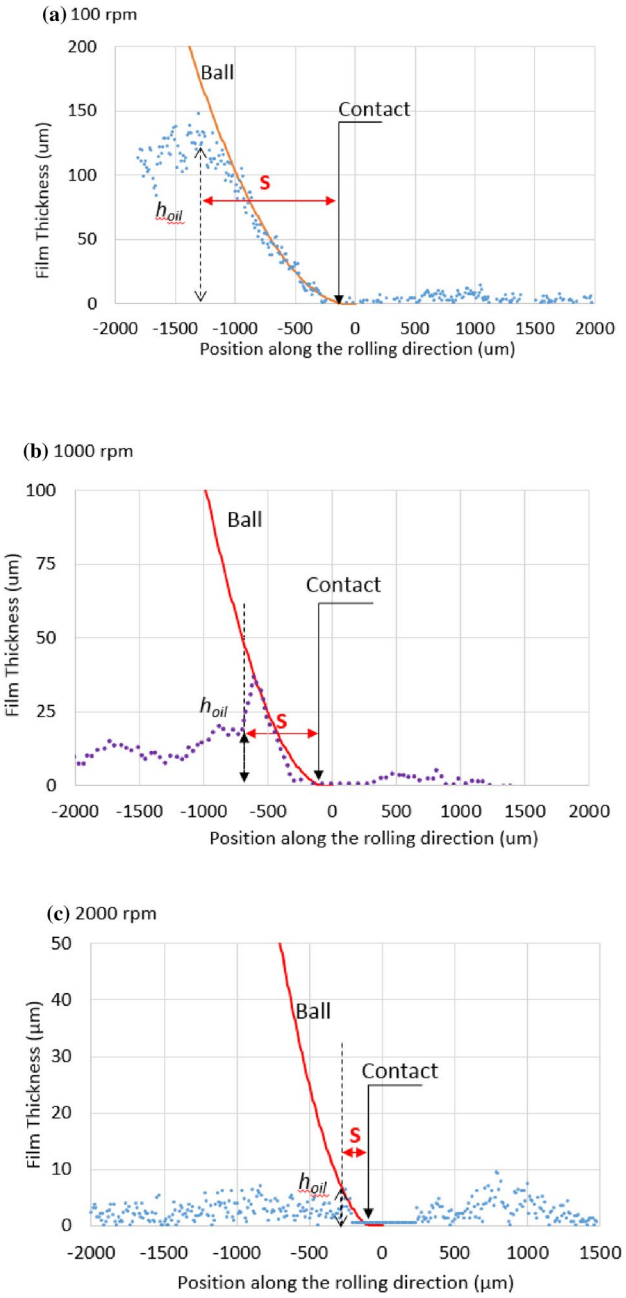

Fig. 9 Film thickness profile and the ball geometry along the centre of contact in the rolling direction for three different bearing speeds extracted from the 3D maps in Fig. 8: **a** 100 rpm, **b** 1000 rpm and **c** 2000 rpm; Oil M1000, Max. Hertz pressure (ball–outer ring contact) = 1.57 GPa, Sump test temperature = 32 °C (Color figure online)

5 Discussion

5.1 Benefits of the Presented Set-Up and Its Potential Applications

This paper presents a novel experimental set-up, referred to as the 'sapphire bearing rig' or 'SBR', that makes it possible

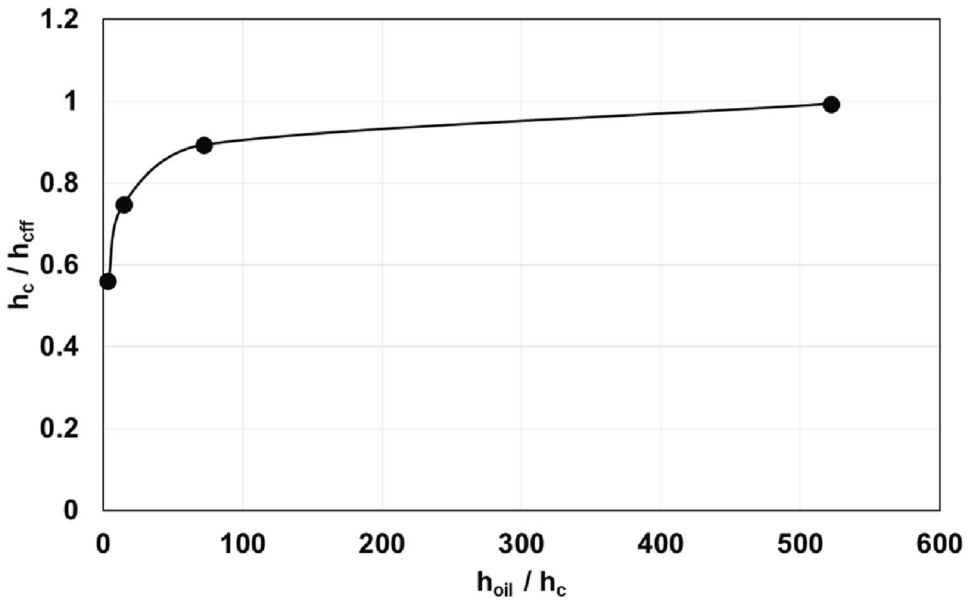

Fig. 10 Plot of ratio of measured central oil film thickness and predicted film using fully flooded EHL theory, h_c/h_{cff}, as a function of the nondimensional thickness of the oil layer in the inlet, h_{oil}/h_c (Color figure online)

for the first time to directly observe and measure the lubricant film thickness in a single element–ring contact in a radially loaded model rolling bearing operating under realistic conditions. In parallel, the set-up is also capable of providing a 3D map of lubricant film in the rolling track around the contact, including the contact inlet, using a novel application of ratiometric laser induced fluorescence technique. This provides knowledge of the inlet oil supply conditions which is crucial in understanding the observed in-contact film thickness. The method provides obvious benefits over other techniques employed for bearing film thickness measurements such as capacitance which provide a measure of average film in all element–ring contacts and are commonly limited to axial bearing loads, and ultrasound which is limited to relatively low bearing speeds [20–22]. None of these alternative techniques provide the lubricant film maps around the contact.

The set-up can be used to evaluate the effect of lubricant properties, bearing operating conditions and bearing geometry, including the type of cage and the type and number of rolling elements, on bearing lubrication. The results can be used to help optimise bearing design but also to validate models of starvation and lubricant flow in bearings.

The presented results illustrate the capabilities of the rig using oil as a lubricant but the set-up can just as easily be utilised to study grease lubrication. Arguably, this is a more important application of the rig given that most rolling bearings are grease lubricated and that grease distribution in a bearing as well as the presence of grease thickener play an important but relatively poorly understood part in bearing lubrication and can cause the in-contact oil films to deviate from EHL theory [40, 41]. Authors have already been using the rig to study grease lubrication and will publish the results of these studies in due course.

5.2 Limitations of the Current Set-Up

Perhaps the most obvious limitation of the current implementation of the sapphire bearing rig is the use of a purely cylindrical outer ring instead of the grooved one as used in real deep groove ball bearings. This limitation does not arise from any physical characteristics of the employed methods but is of practical, manufacturing nature as it is simply very difficult and costly to manufacture the groove in a sapphire ring while still maintaining the required cylindricity and surface quality needed for successful film measurements. This limitation can therefore be overcome with further manufacturing effort and expenditure. The lack of groove is likely to have important effects on the lubrication conditions. The ball–outer ring contact here is much narrower in the transverse direction than is the case with a grooved ring. It is also narrower than the ball–inner ring contact. Both of these factors may influence the flow of oil to and from the rolling track between consecutive ball overrollings and hence the conditions in the inlet of the ball–outer ring contact. This may in turn influence the exact operating conditions at which starvation starts to occur for a given lubricant.

It should be noted that the exact same set-up can be used with a cylindrical roller bearing instead of a deep groove ball bearing, in which case the cylindrical outer ring is an accurate representation of the real bearing geometry. This is out of scope of the present paper, but the authors have also implemented this set-up and successfully obtained relevant results albeit at lower contact pressures. A much higher bearing loads are needed to reach similar Hertz pressures

in roller-ring contact as in the current ball–ring contacts; depending on the exact pressures desired, this may necessitate the upgrade of the loading system. Many of the components in the current loading system were borrowed from the tried-and-tested PCS MTM tribometer to ensure reliability. This limits the maximum load to around 75N in the current implementation of the SBR which is sufficient to ensure representative contact pressures of more than 1.5 GPa in the outer ring contact in the case of a ball bearing as used here. By upgrading the stepper motor and using a stiffer loading arm, it is possible to increase this maximum load so that representative contact pressure could also be obtained with a roller bearing of similar size.

The use of a sapphire ring instead of a steel one changes the wetting characteristics of the bearing which may also affect the supply of oil to the contact. The exact effect of this in the present set-up is unknown but sapphire is commonly used as a material for one of the contacting bodies in the optical interferometry set-ups for lubricant film thickness measurements in single contacts.

5.3 Observed Trends in Oil Film Thickness in and Around the Ball–Ring Contact

Preliminary results presented in this article show that oil film thickness in a ball–ring contact falls below that predicted by the standard EHL theory at certain bearing operating conditions. The point at which this occurs is determined by the product of the oil viscosity and bearing rotational speed. The maps of the oil film in the rolling track ahead of the approaching contact show that this reduction of in-contact film thickness occurs due to a lack of sufficient oil in the rolling track to fully fill the inlet of the approaching contact. This occurs at a given combination of oil viscosity and bearing speed when there is insufficient time for the lubricant to flow back into the rolling track having been pushed away by the passage of the preceding ball.

6 Conclusions

The present paper describes a novel experimental set-up, referred to as the 'sapphire bearing rig' or SBR, for in situ imaging and measurement of lubricant films in a model rolling bearing operating under realistic conditions. Optical access to the region of the element–outer ring contact is afforded by the use of a cylindrical sapphire outer ring. The main features of the set-up are:

- It is able to directly image and measure the film thickness in the element–outer ring contact with accuracy of a few nanometres using an optical interferometry technique.
- It is able to obtain quantitative 3D maps of lubricant film thickness around the contact, including in the rolling track ahead of the contact and hence the immediate contact inlet, with the accuracy of a few microns using a novel application of ratiometric laser induced fluorescence technique.
- The set-up therefore can establish when the in-contact film thickness deviates from that predicted using the EHL theory and in parallel quantify the oil supply conditions in the contact inlet.
- The presented results show that past a certain bearing speed, the in-contact film thickness falls below that predicted by standard EHL theory. The 3D maps of the oil film ahead of the contact show that this reduction in film is caused by the onset of starvation. The conditions at which starvation occurs is shown to depend on the product of lubricant viscosity and bearing rotational speed.
- The set-up can help in optimising lubricant properties, be it oil or grease, and bearing design, for example the type of the bearing cage, to improve bearing lubrication performance.

Appendix

A1. Basic Laser-Induced Fluorescence Imaging

Laser-induced fluorescence (LIF) is a commonly used technique in flow visualisation and investigations [13–16]. It was pioneered more than 40 years ago by Smart and Ford [13] for the studies of oil films between piston ring and cylinder liner. From the early 2000s, LIF saw its gradual adoption as an experimental method in tribology for thin film investigations in compliant contacts starting with the work of Sugimura et al. [42] on a ball-on-disc type configuration. In its basic form, a LIF imaging experiment in fluids consists of dissolving a fluorescent dye in a fluid and subjecting the probed volume to photo-excitation; the resulting fluorescence signal is then collected and imaged on an imaging sensor where the fluorescence power emitted per unit area, S_F, is amplified and converted into pixel intensity values.

For a probe volume of excitation spot area, A, and cross-sectional thickness l, the fluorescence emission intensity I_f per unit area is

$$I_f(l) = I_0\phi(1 - e^{-\epsilon_{\lambda_{ex}} Cl}) \tag{1}$$

The spectral width of fluorescence emission depends the particular dye's photophysical characteristics, the intensity I_f

is a function of the concentration C of the fluorescent species in the fluid, the excitation light intensity I_0 at wavelength λ_{ex} and the probed volume cross-sectional thickness l. The dye's quantum efficiency, ϕ, is the ratio of photons absorbed to the photons emitted through fluorescence and $\varepsilon_{\lambda_{ex}}$ is the molar extinction coefficient, an intrinsic property of the dye.

The excitation light intensity I_0 decays exponentially as it travels through the probe volume according to Eq. (2) with $\frac{I_0}{I_T}$ the ratio between the incident (excitation) I_0 and the transmitted I_T light being:

$$\frac{I_0}{I_T} = e^{-\varepsilon_{\lambda_{ex}} Cl} \tag{2}$$

Equation (2) is normally expressed as Eq. (3) which is also known as the Beer–Lambert law [43]:

$$Abs = \log \frac{I_0}{I} = \varepsilon_{\lambda_{ex}} Cl, \tag{3}$$

where Abs is the probe volume absorbance at wavelength λ_{ex}.

For low absorbances, i.e. $A << 1$, a Taylor series expansion of Eq. (1) leads to:

$$I_f(l) \approx I_0 \phi \varepsilon_{\lambda_{ex}} Cl \tag{4}$$

That is the fluorescent intensity is linearly proportional to the film thickness for weakly absorbing, dilute probe volumes. This relationship is valid for a range of excitation intensities as long as the dye saturation intensity I_{sat} is not exceeded [37], since:

$$I_{ex} = \frac{I_o}{1 + \frac{I_0}{I_{sat}}} \tag{5}$$

It can be seen from Eq. (5), that as long as $I_0 \ll I_{sat}$, the effective excitation intensity I_{ex} is equal to I_o and linearity of relationship in Eq. (4) holds. In LIF experiments, it is critical to always operate in excitation regimes well below the dye's excitation saturation intensity, especially during the calibration step or when operating at short exposures as discussed previously.

The fluorescence signal S_f collected by the imaging sensor over an integration time t and over a range of emission wavelengths between λ_1 and λ_2 ($\lambda_1 < \lambda 2$) can be approximated by:

$$S_f = AKt \int_{\lambda_1}^{\lambda_1} I_f(\lambda) \mathrm{d}\lambda = KAI_0 \phi \varepsilon_{\lambda_{ex}} Clt, \tag{6}$$

where K is an experimental constant which takes into account the various losses that might exist in the setup as well as other optical, electronic and photophysical effects.

Film thickness measurements using LIF are made with the assumption that Eq. (6) is valid i.e. a uniform illumination in space and time with an excitation intensity below I_{sat} impinging on a dilute and weakly absorbing probe volume. A calibration step involves an experiment whereby S_f is correlated to known film thicknesses (h) so that the generated calibration curve can subsequently be used for film thickness determination.

While the validity of this general procedure is well established for a typical ball-on-disc setup, where I_0 is considered constant, this is not the case for the SBR configuration. For the latter, Eq. (6) cannot be assumed valid since during bearing operation, the excitation light incidence angle on the contact zone will change with the spatial position of the ball; this variability compounds with the one due to the temporal instabilities of light source. A further important aspect specific to the SBR is that because the resident time of the contact in the excitation field changes with bearing speed, to keep the I_0 constant every bearing speed would require an adjustment of the excitation light intensity. These factors introduce variability in the excitation intensity, I_0 and therefore the direct use of Eq. (6) for film thickness measurements would produce inaccurate values in the present experiments. To address this, an alternative ratiometric fluorescence approach that does not rely on constant excitation intensity, I_0 was adopted for the present SBR set-up.

A2. Ratiometric Laser Induced Fluorescence Imaging

The ratiometric LIF imaging approach implemented on the SBR uses two fluorescent dyes (a donor and an acceptor) dissolved in a fluid to take advantage of a fluorescence measurement artefact known as the inner-filter effect. This approach is similar to the one proposed by Hidrovo et al. [39], termed Emission Reabsorption Laser Induced Fluorescence (ERLIF).

Although the inner filter effect can occur for a single dye system, it is more pronounced in the case of a mixture of two dyes [38]. This fluorescence quenching effect may occur whenever there is a spectral overlap between the donor dye (D) emission and the acceptor dye (A) absorption spectra so that a radiative transfer process can take place between them whereby a photon emitted by D is absorbed by A. This radiative transfer results in a decrease of the donor quantum efficiency in the region of spectral overlap and hence a decrease in the donor fluorescence signal. The ratiometric imaging consists of separating the donor and acceptor signal and using the ratio as a scalar with no dependence on excitation intensity but only the cross-sectional depth of the probed volume i.e. the oil film thickness in the present case.

Following similar formulation as Valeur [44], for a given concentration C_A and C_D of donor and acceptor dyes in a

fluid, the fraction a of photons emitted by D and absorbed by A is:

$$a = \frac{1}{\phi_D^0}\int_0^\infty I_D(\lambda)\left[1 - e^{-\epsilon_A(\lambda)C_A l}\right]d\lambda, \tag{7}$$

where ϕ_D^0 is the fluorescence quantum yield of the donor in the absence of acceptor and $I_D(\lambda)$, $\epsilon_A(\lambda)$ the donor fluorescence intensity and molar absorption coefficient of the acceptor, respectively.

For dilute and weakly absorbing probe volumes Eq. (7) can be simplified to:

$$a = \frac{C_A l}{\phi_D^0}\int_0^\infty I_D(\lambda)\epsilon_A(\lambda)d\lambda \tag{8}$$

With the magnitude of the spectral overlap between D and A represented by the integral in Eq. (8). The donor fluorescence signal can therefore be expressed as:

$$S_D = S_D^0(1 - a), \tag{9}$$

where S_D^0 is the donor fluorescence signal in the absence of the acceptor.

Using the expression in Eq. (6) and assuming a dilute and weakly absorbing probe volume, the ratio, R, of the donor and acceptor fluorescence signals, $S_D and S_A$ respectively, is:

$$R = \frac{S_D}{S_A} = \frac{S_D^0(1-a)}{S_A} = \frac{\phi_D^0\epsilon_D(\lambda)C_D}{\phi_A\epsilon_A(\lambda)C_A}[1 - \frac{C_A l}{\phi_D^0}\int_0^\infty I_D(\lambda)\epsilon_A(\lambda)d\lambda] \tag{10}$$

If the overlap integral, O, is assumed as invariant for the two fluorescent dyes undergoing radiative transfer, Eq. (10) can be simplified to:

$$R = \frac{\phi_D^0\epsilon_D(\lambda)C_D}{\phi_A\epsilon_A(\lambda)C_A}\left(1 - \frac{OC_A}{\phi_D^0}l\right) = B - Cl, \tag{11}$$

where B and C are constants.

From (11) it follows that the ratio of the fluorescence signals from the donor and acceptor dyes, D and A, correlates linearly with the film thickness, l, with dependence on the excitation intensity I_0 suppressed. This ratiometric approach also has the benefit of suppressing other undesirable setup specific factors that might affect the fluorescence signal such as optical non-linearities and surface reflectivity.

Funding The authors gratefully acknowledge the support of SKF RTD, the Netherlands for the work reported here. The research leading to these results also received funding from the People Programme (Marie Curie Actions) of the European Union's Seventh Framework Programme FP7/2007-2013 under REA Grant Agreement No. 612603.

Declarations

Conflict of interest The authors have not disclosed any competing interest.

Open Access This article is licensed under a Creative Commons Attribution 4.0 International License, which permits use, sharing, adaptation, distribution and reproduction in any medium or format, as long as you give appropriate credit to the original author(s) and the source, provide a link to the Creative Commons licence, and indicate if changes were made. The images or other third party material in this article are included in the article's Creative Commons licence, unless indicated otherwise in a credit line to the material. If material is not included in the article's Creative Commons licence and your intended use is not permitted by statutory regulation or exceeds the permitted use, you will need to obtain permission directly from the copyright holder. To view a copy of this licence, visit http://creativecommons.org/licenses/by/4.0/.

References

1. Ehret, P., Dowson, D.: Past, present and future studies in elastohydrodynamics. Proc. Inst. Mech. Eng. Part J J. Eng. Tribol. **213**, 317–333 (1999)
2. Spikes, H.A.: Thin films in elastohydrodynamic lubrication: the contribution of experiment. Proc. Inst. Mech. Eng. Part J J. Eng. Tribol. **213**, 335–352 (1999)
3. Spikes, H.A.: Sixty years of EHL. Lubr. Sci. **18**, 265–291 (2006)
4. Lugt, P.M., Morales-Espejel, G.E.: A review of elasto-hydrodynamic lubrication theory. Tribol. Trans. **54**, 470–496 (2011)
5. Zhu, D., Jane, W.Q.: Elastohydrodynamic lubrication: a gateway to interfacial mechanics—review and prospect. J Tribol **133**, 041001 (2011)
6. Cameron, A., Gohar, R.: Theoretical and experimental studies of the oil film in lubricated point contact. Proc. Roy. Soc. Lond. **A291**, 520–536 (1966)
7. Johnston, G., Wayte, R., Spikes, H.: The measurement and study of very thin lubricant films in concentrated contacts. Tribol. Trans. **34**, 187–194 (1991)
8. Luo, J., Wen, S., Huang, P.: Thin film lubrication. Part I. Study on the transition between EHL and thin film lubrication using a relative optical interference intensity technique. Wear **194**, 107–115 (1996)
9. Archard, J.F., Kirk, M.T.: Lubrication at point contacts. Proc. R. Soc. Lond. Ser. A Math. Phys. Sci. **261**(1307), 532–550 (1962)
10. Wilson, A.: The relative thickness of grease and oil films in rolling bearings. Proc. Inst. Mech. Eng. **193**, 185–192 (1979)
11. Dwyer-Joyce, R., Drinkwater, B., Donohoe, C.: The measurement of lubricant–film thickness using ultrasound. Proc. R. Soc. Lond. A Math. Phys. Eng. Sci. **459**, 957–976 (2003)
12. Dwyer-Joyce, R., Harper, P., Drinkwater, B.: A method for the measurement of hydrodynamic oil films using ultrasonic reflection. Tribol. Lett. **17**, 337–348 (2004)
13. Smart, A., Ford, R.: Measurement of thin liquid films by a fluorescence technique. Wear **29**, 41–47 (1974)
14. Hoult, D.P., Lux, J.P., Wong, V.W., Billian, S.A.: Calibration of laser fluorescence measurements of lubricant film thickness in engines. SAE Technical Paper (1988)
15. Myant, C., Reddyhoff, T., Spikes, H.A.: Laser-induced fluorescence for film thickness mapping in pure sliding lubricated, compliant, contacts. Tribol. Int. **43**, 1960–1969 (2010)
16. Fowell, M.T., Myant, C., Spikes, H.A., Kadiric, A.: A study of lubricant film thickness in compliant contacts of elastomeric seal

materials using a laser induced fluorescence technique. Tribol. Int. **80**, 76–89 (2014)
17. Glovnea, R.P., Forrest, A.K., Olver, A.V., Spikes, H.A.: Measurement of sub-nanometer lubricant films using ultra-thin film interferometry. Tribol. Lett. **15**, 217–230 (2003)
18. Luo, J., Shen, M., Wen, S.: Tribological properties of nanoliquid film under an external electric field. J. Appl. Phys. **96**, 6733–6738 (2004)
19. Reddyhoff, T., Choo, J.H., Spikes, H.A., Glovnea, R.P.: Lubricant flow in an elastohydrodynamic contact using fluorescence. Tribol. Lett. **38**, 207–215 (2010)
20. Dwyer-Joyce, R.S., Reddyhoff, T., Drinkwater, B.W.: Operating limits for acoustic measurement of rolling bearing oil film thickness. Tribol. Trans. **47**, 366–375 (2004)
21. Wan Ibrahim, M.K., Gasni, D., Dwyer-Joyce, R.S.: Profiling a ball bearing oil film with ultrasonic reflection. Tribol. Trans. **55**(4), 409–421 (2012)
22. Li, M., Jing, M., Chen, Z., Liu, H.: Ultrasound measurement of lubricant-film thickness distribution in cylindrical roller bearings. In: 2013 IEEE International Symposium on Assembly and Manufacturing (ISAM), pp. 304–306. IEEE, Xi'an (2013)
23. Jablonka, K., Glovnea, R., Bongaerts, J.: Evaluation of EHD films by electrical capacitance. J. Phys. D Appl. Phys. **45**(38), 385301 (2012)
24. Morales-Espejel, G.E., Lugt, P.M., Pasaribu, H.R., Cen, H.: Film thickness in grease lubricated slow rotating rolling bearings. Tribol. Int. **74**, 7–19 (2014)
25. Jablonka, K., Glovnea, R., Bongaerts, J.: Quantitative measurements of film thickness in a radially loaded deep-groove ball bearing. Tribol. Int. **119**, 239–249 (2018)
26. Safa, M.M.A., Anderson, J.C., Leather, J.A.: Transducers for pressure, temperature and oil film thickness measurement in bearings. Sens. Actuators **3**, 119–128 (1982)
27. Bahadoran, H., Gohar, R.: Oil film thickness in lightly-loaded roller-bearings. J. Mech. Eng. Sci. **16**, 386–390 (1974)
28. Ohno, N., Tanimoto, K., Kuwano, N., Hirano, F.: Effect of the base oil viscosity of lithium soap greases on life of thrust ball bearings. Jpn. J. Tribol. **43**, 1545–1556 (1998)
29. Wedeven, L.D., Evans, D., Cameron, A.: Optical analysis of ball bearing starvation. J. Lubr. Technol. **93**, 349–361 (1971)
30. Barker, D.C., Johnston, G.J., Spikes, H.A., Bünemann, T.: EHD film formation and starvation of oil in water emulsions. Tribol. Trans. **36**, 565–572 (1993)
31. Chevalier, F., Cann, P., Colin, F., Dalmaz, G., Lubrecht, A.: Film thickness in starved EHL point contacts. J. Tribol. **120**, 126–133 (1998)
32. Damiens, B., Venner, C.H., Cann, P.M.E., Lubrecht, A.A.: Starved lubrication of elliptical EHD contacts. J. Tribol. **126**, 105 (2004)
33. Svoboda, P., Kostal, D., Krupka, I., Hartl, M.: Experimental study of starved EHL contacts based on thickness of oil layer in the contact inlet. Tribol. Int. **67**, 140–145 (2013)
34. Poll, G., Li, X., Bader, N., Guo, F.: Starved lubrication in rolling contacts—a review. Bear. World J. **4**, 69–81 (2019)
35. Noda, T., Shibasaki, K., Wang, Q.J.: X-Ray CT Imaging of Grease Behavior in Ball Bearing and multiscale grease flows simulation. STLE Annula Meeting 2016, Las Vegas, US, May 2016
36. Franken, M.J.Z., Chennaoui, M., Wang, J.: Mapping of grease migration in high-speed bearings using a technique based on fluorescence spectroscopy. Tribol. Trans. **60**(5), 789–793 (2017)
37. Patsayeva, S.V., Yuzhakov, V.I., Varlamov, V.: Laser-induced fluorescence saturation for binary mixtures of organic luminophores. In: ICONO'98: Laser Spectroscopy and Optical Diagnostics: Novel Trends and Applications in Laser Chemistry, Biophysics, and Biomedicine: International Society for Optics and Photonics, pp. 147–156. SPIE, Bellingham (1999)
38. Jones, A.C., Millington, M., Muhl, J., De Freitas, J., Barton, J.S., Gregory, G.: Calibration of an optical fluorescence method for film thickness measurement. Meas. Sci. Technol. **12**, N23 (2001)
39. Hidrovo, C.H., Hart, D.P.: Emission reabsorption laser induced fluorescence (ERLIF) film thickness measurement. Meas. Sci. Technol. **12**, 467–477 (2001)
40. Kanazawa, Y., De Laurentis, N., Kadiric, A.: Studies of friction in grease-lubricated rolling bearings using ball-on-disc and full bearing tests. Trib. Trans. **63**(1), 77–89 (2020)
41. Lugt, P.M.: Grease lubrication in rolling bearings. Wiley, Hoboken (2012)
42. Sugimura, J., Hashimoto, M., Yamamoto, Y.: Study of elastohydrodynamic contacts with fluorescence microscope. Tribiol. Ser. **38**, 609–617 (2000)
43. Swinehart, D.F.: The beer-lambert law. J. Chem. Educ. **39**, 333 (1962)
44. Valeur, B.: Molecular fluorescence. In: Digital Encyclopedia of Applied Physics, pp. 477–531. Wiley, Weinheim (2003)

Publisher's Note Springer Nature remains neutral with regard to jurisdictional claims in published maps and institutional affiliations.